Consequences of a Solar Wind Stream Interaction Region on the Low Latitude Ionosphere: Event of 7 October 2015

M.G. Molina[1,2,3] · **S. Dasso[4,5]** · **G. Mansilla[5,6]** ·
J.H. Namour[1] · **M.A. Cabrera[2]** · **E. Zuccheretti[7]**

Abstract In this article, we present a study of the perturbations occurring in the Earth's environment on 7 October 2015. We use a multi-instrument approach, including space and ground observations.

In particular, we study the ionospheric conditions at low latitudes. Two ionospheric storms are observed at the low latitude station of Tucumán (26° 51′ S, 65° 12′ W). We observe a negative ionospheric storm followed by a positive one. These ionospheric perturbations were triggered by two sudden storm commencements (SSCs) of a strong geo-

✉ M.G. Molina
  gmolina@herrera.unt.edu.ar

  S. Dasso
  sdasso@iafe.uba.ar

  G. Mansilla
  gmansilla@herrera.unt.edu.ar

  J.H. Namour
  jnamour@herrera.unt.edu.ar

  M.A. Cabrera
  mcabrera@herrera.unt.edu.ar

  E. Zuccheretti
  enrico.zuccheretti@ingv.it

1 Laboratorio de Computación Científica, Departamento de Ciencias de la Computación, Facultad de Ciencias Exactas y Tecnología (FACET), Universidad Nacional de Tucumán (UNT), Av. Independencia 1800, Tucumán, Argentina

2 Laboratorio de Telecomunicaciones, FACET, UNT, Av. Independencia 1800, Tucumán, Argentina

3 CONICET, UNT, Av. Independencia 1800, Tucumán, Argentina

4 Facultad de Ciencias Exactas y Naturales, Departamento de Ciencias de la Atmósfera y los Océanos y Departamento de Física, Universidad de Buenos Aires, Intendente Güiraldes 2160, Ciudad Universitaria, C1428EGA Ciudad Autónoma de Buenos Aires, Argentina

magnetic storm. Preliminary results show that the main mechanism involved in both iono-spheric storms is the prompt penetration of electric fields (PPEFs) from the magnetosphere. Furthermore, in the positive storm, disturbed dynamo electric fields are observed acting in combination with the PPEFs. The impact of the solar wind on the Earth's environment is analyzed using geomagnetic data and proxies, combined with data acquired in the Tucumán Low Latitude Observatory for the Upper Atmosphere.

We also investigate the solar and interplanetary drivers of this intense perturbation. We find that, although typically interplanetary coronal mass ejections (ICMEs) are the most geo-effective transient interplanetary events, in this case, a corotating interaction region (CIR) is responsible for these strong perturbations to the geospace.

Keywords Ionospheric storm · Low latitude ionosphere · Solar wind · Corotating interaction region

1. Introduction

Space weather events can be initiated by solar events (e.g., solar flares or solar transient perturbations affecting the solar wind conditions) or by tropospheric dynamical processes (e.g., gravity waves) (see Prölss, 2004).

Two major space weather interplanetary drivers are interplanetary coronal mass ejections (ICMEs) (e.g. Retterer and Kelley, 2010) and corotating interaction regions (CIRs) (e.g. Richardson, 2018; Grandin, Aikio, and Kozlovsky, 2019). These two classes of events are interplanetary transients, originating in the Sun. ICMEs are the interplanetary counterpart of coronal mass ejections (CMEs) which can be remotely observed in white-light coronagraph images. CIRs are consequences of the interaction of fast solar wind streams originating in solar coronal holes (CHs) with slower interplanetary plasma; this interaction typically produces perturbations to interplanetary conditions that can cause significant effects on the geospace. In particular, these transient events can drive interplanetary shocks, accelerate particles, modulate the flux of galactic cosmic rays, and produce magnetic and ionospheric storms in the space environment of planets. Thus, the passage of ICMEs and CIRs near Earth can produce geomagnetic and ionospheric storms, which can be observed by different terrestrial ground instruments. In particular, several key solar wind properties can be used to model the level of coupling between the solar wind and the magnetosphere (e.g. Newell et al., 2007).

In this work, we study the intense geomagnetic storm occurring on 7 October 2015, its consequences on the low latitude ionosphere, and its main solar and interplanetary driver. The solar wind conditions triggered an intense geomagnetic storm with consequences on the ionosphere. We are especially interested in the ionospheric response at low latitudes, and we analyze the consequences over Tucumán station (26° 51′ S, 65° 12′ W).

We study the CIR event and the solar wind-magnetosphere-ionosphere coupling using a multi-instrument approach with emphasis in the ionosphere at the mentioned low latitude

[5]   Instituto de Astronomía y Física del Espacio, CONICET, Universidad de Buenos Aires, Intendente Güiraldes 2160, Ciudad Universitaria, C1428ZAA, Ciudad Autónoma de Buenos Aires, Argentina

[6]   Departamento de Física, FACET, UNT, Av. Independencia 1800, Tucumán, Argentina

[7]   Istituto Nazionale di Geofisica e Vulcanologia (INGV), Via di Vigna Murata 605, 00143 Rome, Italy

station. This approach, within the last years, has been used by many authors to address this complex and large domain (see, e.g., Dasso and Shea, 2020).

It is well known that during magnetic storms, a significant amount of energy is transferred from the solar wind to the magnetosphere. The auroral region is one of the regions presenting strong coupling between the interplanetary medium, the magnetosphere, the thermosphere, and the ionosphere. From the auroral region to lower latitudes several mechanisms can trigger a variety of phenomena.

Consequences within the Earth's ionosphere due to geomagnetic storms are quite different according to the ionospheric region in question. High variability in the ionosphere can be observed both, in space and in time. Its morphology varies according to the geographical and geomagnetic location, and also according to daily and seasonal characteristics and to the solar cycle. This variability affects propagation via the ionosphere with a high impact in telecommunications, which can be critical during extreme space weather events (Zolesi and Cander, 2014).

Also, at different ionospheric heights (or ionospheric regions) distinct physical mechanisms govern the changes in the electron concentration. Thus, the reaction of each region to a geomagnetic storm will vary. On one hand, at the lower ionosphere (E and D region), the response (post-storm effects, auroral absorption, polar cap absorption (PCA)) can be observed as an increment when compared to a background level. Meanwhile in the F2 region the difference in ionization due to a reaction to the geomagnetic storm can be observed as an enhancement (positive sign) or as a depletion (negative sign) called ionospheric storms (Danilov, 2013).

Ionospheric storms can last from some hours to days, during this period the band of available frequencies for radio-wave propagation through the ionosphere is reduced and, in extreme cases, can be completely blocked out in some regions. Ionospheric storms can be observed as disturbances in density distribution, total electron content, and the current system. Ionospheric storms (in the F region) are large disturbances with origin in the coupling between the solar wind and the magnetosphere. This complex coupling occurs due to solar wind energy dissipation into the auroral ionosphere where it triggers changes in composition, electric fields, winds, and temperature (Zolesi and Cander, 2014).

As mentioned above the ionospheric behavior changes, also, substantially latitudinally. The equatorial ionosphere behavior, in particular its F region, can be singular when compared to other latitudes. At the geomagnetic Equator, the Earth's magnetic field is horizontal while the Sun affects the atmosphere perpendicularly. As a result, a significant ionization vertical drift appears caused by the electric and magnetic field combination. The reason is that, at the Equator, the magnetic field, B, is almost parallel to the Earth's surface and the E region dynamo electric field, E, is eastward (at daytime). Thus, the $E \times B$ drift produces an upward plasma transport at the F region (at the Equator). This plasma is later transported along the magnetic field lines due to the gravity and pressure-gradient forces. The described mechanism forms an anomaly of ionization (at equatorial latitudes) consisting of a region of minimum ionization density at the magnetic equator and in two crests of maximum ionization density at low latitudes (near $5° - 20°$ in magnetic latitude), both to the south and north. This phenomenon is known as the equatorial ionization anomaly (EIA) and the electrodynamic mechanism is called the equatorial "fountain effect" (see Kelley, 1989; Zolesi and Cander, 2014; among others).

In this article, we are interested in the consequences on the ionosphere over Tucumán Province in Argentina of the strong geomagnetic storm of 7 October 2015. The Tucumán Low Latitude Observatory for the Upper Atmosphere (26° 51′ S, 65° 12′ W) is located near the south crest of the EIA (its dip latitude is $\approx 15°$) and so, its ionization during the day is

significantly higher than in other latitudes. Another interesting characteristic of Tucumán is that it is also located close to the South Atlantic Magnetic Anomaly.

The 7 October 2015 strong geomagnetic storm was studied by Matsui et al. (2016) to analyze a dipolarization event in the inner magnetosphere. They investigated this event because, in the magnetotail, burst bulk flows toward the Earth are often accompanied by dipolarization signatures. In particular, they observed the dipolarization event within the interval 23:35 – 23:50 UT measured in the inner magnetosphere combining multispacecraft data. As the authors stated, more measurements for different cases should be analyzed in the future to detect and study such dipolarization events. This kind of measurement and analysis in comparison with ionospheric data can be useful for a more detailed comprehension about the magnetosphere-ionosphere coupling.

This article is organized as follows. In Section 2 we present the instruments and data sets that have been used in this study. Section 3.1 explains the solar driver and magnetosphere coupling for this event and Section 3.2 analyzes the ionospheric response at the low latitude station of Tucumán. Besides, Section 3.2.1 deals with the analysis of the negative ionospheric storm and Section 3.2.2 with that of the positive ionospheric storm. Section 4 discusses the results and summarizes the main conclusions.

2. Observations and Instruments

The data used to identify the probable solar source of the geomagnetic storm consist of 193 Å images obtained by the Atmospheric Imaging Assembly (AIA) onboard the Solar Dynamics Observatory (SDO).

To analyze the interplanetary conditions near Earth, we used data acquired with the Advanced Composition Explorer (ACE) spacecraft. We analyzed, in particular, the total interplanetary magnetic field (IMF) magnitude, Bt, and its southward component, Bz, both measured in nT in the geocentric solar magnetospheric (GSM) coordinate system. We also studied the solar wind speed, temperature, and density, obtained from http://omniweb.gsfc.nasa.gov/, and we included the induced electric field.

In the magnetosphere, we analyzed the Dst index provided by the World Data Center for Geomagnetism, Kyoto (http://wdc.kugi.kyoto-u.ac.jp), as the proxy for the geomagnetic activity.

To study the ionospheric response we processed data from instruments at the Tucumán Low Latitude Observatory for the Upper Atmosphere at the National University of Tucumán. We observed the ionosphere using: (a) an ionospheric sounder mainly to analyze the critical frequency of the F2 layer and (b) a GPS receiver system to observe the total electron content (TEC).

The ionospheric sounder is an AIS-INGV system operative at the observatory since 2007. The system obtains the virtual height of the ionosphere for a frequency span using the so-called vertical sounding technique. The instrument uses high frequency (HF) radio waves reflecting in the ionospheric plasma and measures the time delay of the echo of these reflected radio waves. Then the virtual height of the ionospheric layers can be calculated and the resulting profile or ionogram can be obtained. The interpretation of the ionograms (or scaling) allows for obtaining one of the most important parameters, that is, the critical frequency of the F2 layer, *foF2*. The *foF2* is the frequency relative to the maximum reflectivity of the ionosphere and is related to the highest electron density (Bianchi et al., 2013; Cabrera et al., 2010; Molina et al., 2016).

The ionograms used in this work were automatically scaled and later manually corrected. In order to obtain the reference curve for comparison between geomagnetically disturbed and non-disturbed cases, we performed an hourly averaged curve using five geomagnetically quiet days. Because of data availability, and according to the reported geomagnetically quiet days (http://wdc.kugi.kyoto-u.ac.jp/qddays/index.html), we considered the time period 26–30 September 2015 to compute the reference curve. These geomagnetically quiet days have been used also to compare the TEC on the storm days against its reference curve.

Another magnitude of interest, derived from the ionosonde, is $hmF2$ which is the height of the maximum electron density of the F2 layer. The $hmF2$ value can be roughly computed using the Shimazaki formula (Shimazaki, 1955):

$$hmF2 = 1490/(M\,(3000)\,F2) - 176 \text{ km},\qquad(1)$$

where $M(3000)F2$ (also known as the transmission factor M) can be obtained from scaled ionograms. The $M(3000)F2$ is related to the maximum usable frequency (MUF) for an oblique propagation distance of 3000 km, and to $foF2$ as follows (Zolesi and Cander, 2014):

$$M\,(3000)\,F2 = \frac{MUF\,(3000)\,F2}{foF2}.\qquad(2)$$

In this study, the $M(3000)F2$ values have been obtained from the auto-scaled values within the ionograms of the AIS-INGV system.

Several authors have improved the Shimazaki formula to quantify better the $hmF2$ by replacing the constants 1490 and 176 km with other values. Later, Bradley and Dudeney (1973) introduced an additional parameter having in mind the E region ionization. Until 1972, the dependence on solar activity had not been considered in the $hmF2$ calculation until the time when Eyfrig introduced also the R12 index (Bilitza, Sheik, and Eyfrig, 1979). We are interested in the behavior of the ionosphere (in height) more than in its proper quantification, and thus the Shimazaki formula is sufficient, and can be easily and automatically derived from scaled ionograms.

The F2-layer response to geomagnetic perturbations is, in general, described using $\delta foF2$ where

$$\delta foF2 = \frac{foF2\,(obs) - foF2\,(med)}{foF2\,(med)},\qquad(3)$$

$foF2(obs)$ corresponds to the observations and $foF2(med)$ to the corresponding median value in the reference curve.

We also included $vTEC$ (vertical total electron content) derived from measurements at a GPS station in Tucumán. Data have been obtained from the Red Argentina de Monitoreo Satelital Continuo (RAMSAC). Data are publicly available at www.ign.gob.ar. Receiver Independent Exchange Format (RINEX) files can be directly downloaded and, in this case, data from TUCU $(-26°\ 50'\ 35.71836'',\ -65°\ 13'\ 49.26570'')$ station have been used. In order to obtain $vTEC$ in TEC units (TECu) from the RINEX files, the Gopi calibration software tool has been used (see Krishna 2020). TEC is not a direct measurement, which is why the calibration procedure has been applied.

Finally, we added the estimation of the equatorial electric field, EEF, modeled by the Prompt Penetration Equatorial Electric Field Model (PPEEFM) (https://geomag.colorado.edu/real-time-model-of-the-ionospheric-electric-fields.html). This model is based on the relationship between the interplanetary electric field, IEF, and the EEF which is linear. The solar wind electric field can be estimated as $IEF = -V \times B$, where V is the solar wind speed

and B is the solar wind magnetic field. The prompt penetration of solar wind electric fields has an almost immediate impact on the magnetosphere and ionosphere. Data from ACE satellite, radar data from the Jicamarca Unattended Long-term Investigations of the Ionosphere and Atmosphere (JULIA), and the magnetometer in the Challenging Minisatellite Payload (CHAMP) satellite have been used in the model.

3. Data Analysis

3.1. Solar Driver and Magnetosphere Coupling

It is well known that the Sun is the main driver of space weather events. In particular, solar conditions are the cause of fast and slow solar wind streams, corotating interaction regions (CIRs), flares, coronal mass ejections and their interplanetary counterparts (ICMEs), and solar energetic particle event (Bothmer, Zhukov, and Daglis, 2007).

When a fast stream of interplanetary plasma encounters a slow plasma region in its front, an interacting region is formed (the so-called corotating interaction region or CIR, also known as stream interaction region or SIR). The solar source of these fast solar wind streams are coronal holes (CH). Because CHs can be long-living solar structures, which can persist even for many months, CIR regions can be observed at regular intervals of ≈ 27 days viewed from Earth due to solar rotation (e.g. Richardson, 2018).

The main physical reason of CIRs turning the solar wind into geoeffective is the compression of plasma and magnetic field, which is intensified and perturbed during the interaction between the fast and the slow solar wind. This process can be analyzed from the bulk velocity solar wind profile, observed in situ by a spacecraft near Earth. Thus, from several decades a significant correlation was found between the solar wind velocity and the geomagnetic indices (Snyder, Neugebauer, and Rao, 1963).

Typically, CIRs can produce weak to moderate geomagnetic storms (e.g. Tsurutani et al., 2006). Approximately 80% of geomagnetic storms associated with "pure" CIRs (i.e. not associated with CIR-ICME in interaction) are weak ($-50 < \text{Dst} \leq -30$ nT, being Dst the disturbance storm time index) to moderate ($-100 < \text{Dst} \leq -50$ nT), according with the results of Zhang, Richardson, and Webb (2008). On the another hand, Alves (2006) showed that only about 33% of CIRs are associated with moderate to intense storms (Dst ≤ -100 nT). But the most intense geomagnetic storms are mostly associated with CIRs in interaction with ICMEs (Chi et al., 2018). Although CIRs can be observed frequently during the solar minimum phase, they typically produce a lower number of geomagnetic storms mainly due to the fact that they generally present lower speed gradients, lower dynamical pressure peaks, and lower IMF magnitude (Kilpua, Koskinen, and Pulkkinen, 2017). However, due to the low number of ICMEs during a solar minimum, almost 50% of the larger storms occurring during a solar minimum originate from CIRs (Richardson and Cane, 2012; Grandin, Aikio, and Kozlovsky, 2019).

The geoeffectiveness of CIR or SIR/high-speed-stream (HSS) events have been studied from a statistical point of view (from 1995–2017) by Grandin Grandin, Aikio, and Kozlovsky (2019) to obtain an automatic event detection algorithm. This method uses the Richardson and Cane (2010) list of ICMEs as a primary catalog (http://www.srl.caltech.edu/ACE/ASC/DATA/level3/icmetable2.htm), but it filters cases, from the analysis of time derivatives of the intensity of the interplanetary magnetic field and bulk velocity of the solar wind, to remove non-clearly identified ICMEs that produce CIR-ICME interacting regions. After applying the proposed algorithm the authors presented a list of possible pure SIR/HSS events in which, our event of interest (6–8 October 2015) was included.
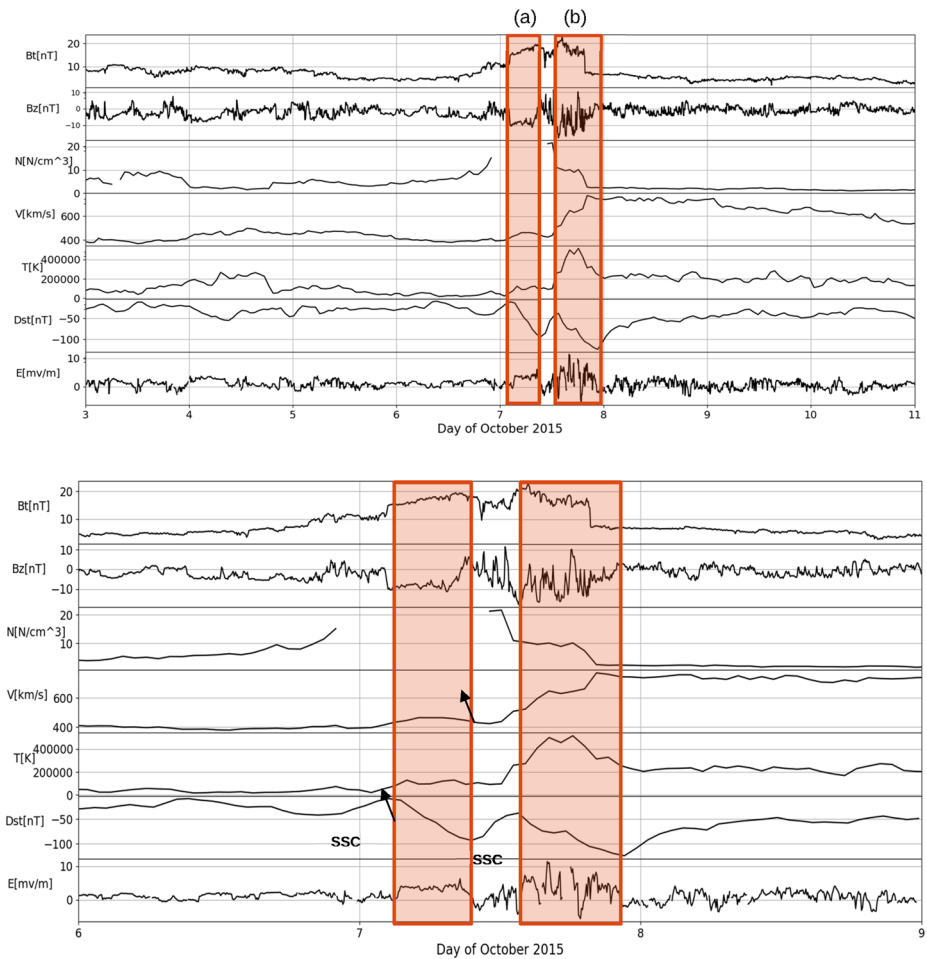
Figure 1 Global parameters of the geomagnetic storm. Panels show (from top to bottom): total IMF Bt, Bz IMF component; solar wind density (N); solar wind density, N; solar wind bulk speed, V; solar wind temperature, T; Dst index; and induced electric field, E. Shadowed regions called (**a**) and (**b**) are marked according to the main phases of the storms, see the references in the Dst panel. Also, in the zoomed panel shown below (6 – 9 October) both storm sudden commencements (SSCs) are marked in the Dst panel. The first SSC occurs at 02 UT (-9 nT) and the second SSC happens at 13 UT (-38 nT).

The Maris Muntean et al. catalog (http://www.geodin.ro/varsiti/2015-2/) also listed our event, but in this case the authors' list contains pure SIR/HSS events and correspond to (or are contaminated by) ICMEs (compared to the Richardson and Cane list).

The arrival of the interplanetary driver to the space environment of Earth is observed during 7 October (see Figure 1), with an interplanetary plasma bulk velocity reaching almost 800 km/s. Thus, considering the Sun-Earth distance and an approximate constant solar wind bulk velocity during most of the travel from the Sun to the terrestrial environment, the travel time can be estimated as ≈ 2.3 days, so that the launching time of solar wind plasma can be estimated between the beginning or middle of 5 October. Figure 2 shows observations obtained from the Atmospheric Imaging Assembly (AIA) images, on board the Solar Dynamics Observatory (SDO), corresponding to 3 – 5 October 2015 (data from

Figure 2 This figure shows an AIA 193 Å image acquired by SDO corresponding to 5 October 2015. The coronal hole near the Sun's equator can be observed facing Earth. This coronal hole is a good source candidate for the intense geomagnetic storm on 7 October 2015. Data source: www.solarmonitor.org.
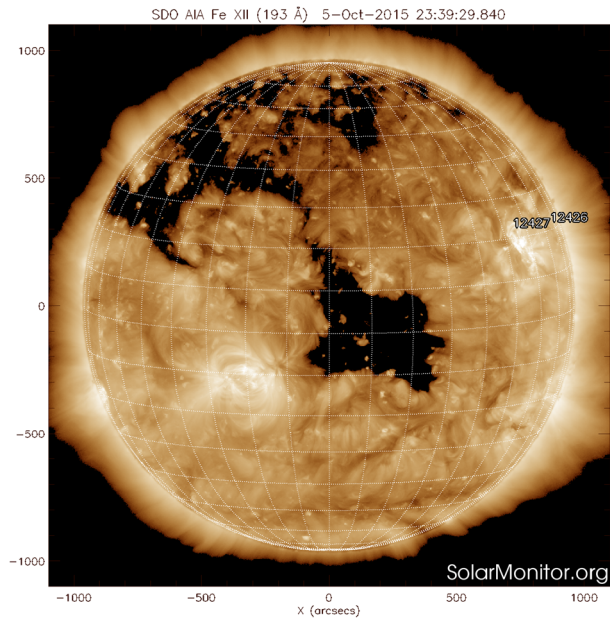
www.solarmonitor.org), showing the Sun at a wavelength of 193 Å. Coronal holes can be observed as dark (black) regions. In this case, the image shows that a huge coronal hole was present during that time, at an equatorial latitude and facing Earth. Thus, we confirm that the structure driving the geomagnetic and ionospheric disturbances analyzed in this article originates in a solar CH, producing a CIR in the interplanetary space.

The bottom panels of Figure 1 show a 3-day zoomed range of the interplanetary properties near Earth, from 6 to 8 of October 2015. From the upper to the lower panels, this figure shows the absolute value of the IMF, its z-component in GSM coordinates, the solar wind proton density, the solar wind temperature, the Dst index, and the induced electric field. In particular, two-time ranges are marked, (a) and (b). These two zones are marked following the Dst curve (see explanation below) that shows the evolution of the storm. A first storm, marked with (a), in the early hours of 7 October is followed, after a brief recovery interval, by a second storm (b) that lasts until the last hours of that day. The presence of these two storms is associated with two sub-structures of the IMF intensity (see upper panel of Figure 1). These sub-structures (i.e. the presence of this double peak of the IMF), could be a consequence of the not so simple shape of the CH that originate it (the CH located near the solar equator; see Figure 2) or could be a consequence of other local processes in the solar wind, for instance some dynamical evolution of the CIR. We cannot conclude what is the detailed reason of finding this double peaked IMF (one single CIR with sub-structure or two CIRs). Before the beginning of region (a), from the end of 6 October to the beginning of 7 October, it is possible to see a gradual increase of B from ≈ 5 nT to ≈ 10 nT. At beginning of region (a) which corresponds to 7 October at 02 UT, there is a jump of B reaching ≈ 20 nT together with an abrupt decrease of Bz, and it is found that at the same time the velocity increases from ≈ 400 km/s to 450 km/s. The temperature has also a small increase not showing clear signatures of discontinuity, as expected in the forward shock formed at the beginning of the CIRs. The behavior of the proton mass density cannot be fully analyzed due to a data gap during this range, but it is observed that it starts to increase before the end of 6 October, just when before the data gap starts. All these observations could be the

consequence of the starting process of formation of the interacting region with a very weak or even in formation forward shock.

At the end of this interacting region (i.e. end of region (b)), it can be observed that the velocity of the solar wind reached a stable value of almost ≈ 800 km/s, and at this time it is possible to see the discontinuity of B and of the proton density, decreasing in time, clear signatures of a reverse shock ending the CIR. The IMF returns to the previous values of 5 nT, before the CIR. Beyond this reverse shock, the proton density presents low values consistent with a rarefaction at the trailing edge.

Thus, we conclude that between the beginning of (a) and the end of (b), a region is found formed due to the interaction between the fast and slow solar wind, within which is a compressed zone with increased (in magnitude) and distorted/irregular (in direction) magnetic field and enhanced mass density (not observed all the time because of the data gap). We note that there are two sub-structures ((a) and (b)); however, the expected increase in temperature due to the compression is only observed in (b). This rough global structure was also observed (not shown here) repeatedly in the solar wind near Earth, lagging 27 days during several solar rotations, which re-enforces the interpretation of a CIR as solar wind driver for the ionospheric perturbation analyzed in this article.

When Bz turns to be negative (see Figure 1) at the first discontinuity, it reaches and keeps a value of -10 nT during several hours, producing the first trigger of a geomagnetic storm as can be seen in Dst, which starts to decrease up to a value of ≈ -93 nT at 10 UT. Thus, a first SSC is observed at 02 UT on 7 October and after that, the main phase of a geomagnetic storm begins until 10 UT, when Dst reaches -93 nT. Later, in agreement with a change of the sign to Bz positive, a recovery phase starts and the value of Dst increases. During phase (b), Bz turns to be negative again (some oscillations can be observed, but it remains mostly negative) and consequently Dst starts to decrease again, re-starting shortly a new SSC at 15 UT when Dst $= -38$ nT (i.e. a two-phase geomagnetic storm, e.g. Kamide et al., 1998), reaching a second Dst peak of -124 nT at 22 UT, when Bz changes of sign toward a positive value. Of course, the combination of Bz with the velocity is the physical forcing, which can be observed in the bottom panel as the induced electric field with decreasing Dst when $E > 0$.

Thus, this interplanetary structure, originating in a solar coronal hole, and developing interplanetary shocks in a complex solar wind stream interaction, was the cause of an intense geomagnetic storm (Dst < -100 nT) and consequently strong perturbations to the ionosphere, as will be described in the next sections.

3.2. Ionospheric Response over Tucumán

Often combined mechanisms are involved in the solar wind-magnetosphere coupling which significantly alter the electron density at low latitudes and the equatorial electrodynamics (Tsurutani et al., 2004; Mannucci et al., 2005; Bagiya et al., 2011). These mechanisms are: the prompt penetration of electric fields (PPEF) with effects on a relatively short period of time (Nishida, Iwasaki, and Nagata, 1966; Kelley, Fejer, and Gonzales, 1979; Gonzales et al., 1979; Fejer, Kamide, and Slavi, 1986; Kikuchi et al., 2000), the ionospheric disturbance dynamo electric field (DDE) with long-lasting effects (Blanc and Richmond, 1980), and finally, the traveling atmospheric disturbance (TAD) and thermospheric composition (O/N2) changes as a result of ionospheric winds (Fuller-Rowell et al., 1997, 2002, 2013).

Geomagnetic storm effects in the ionosphere are difficult to analyze and more difficult to predict, and in some cases, these effects from the geomagnetic storm can be attenuated due to local or regional ionospheric events resulting in less (or none) evident effects on ionospheric measurements.
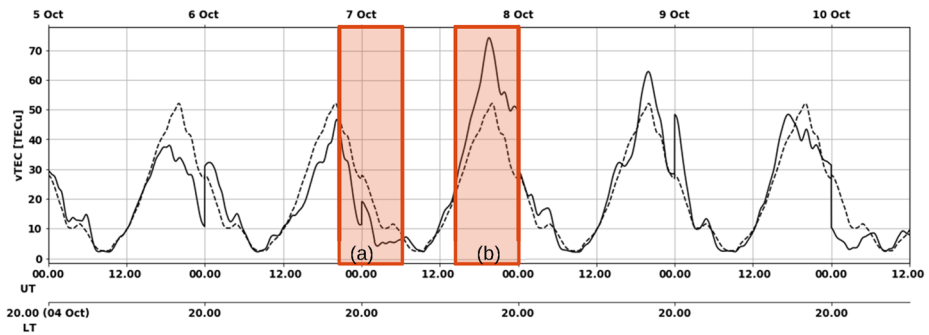
Figure 3 *vTEC* obtained from TUCU GPS station (26° 50′ S, 65° 13′ W) from the RAMSAC network. *vTEC* parameters (bold line) are compared with the reference curve (dashed lines) calculated using the five nearest geomagnetically quiet days.

Moreover, the behavior of the main parameters of the ionosphere, such as $f0F2$ and TEC, during and before a geomagnetic storm is the combined result of several processes. The origin of the acting processes can come from outside, such as the interaction with the interplanetary medium, magnetosphere, and the radiation belts, or they can be originating from below (e.g. thermospheric gas heating, thermospheric winds, and TADs) (Danilov, 2013).

The main features of ionospheric storms have been determined using an ionosonde at mid-latitudes to measure *foF2* and $h'F2$ (height of F2 layer) and also by trans-ionospheric radio-wave propagation to measure TEC. Significant differences in *foF2* and TEC (both positive and negative), when compared to reference curves, are indications of important disturbances in the electron density in the F region. A significant decrease in the ionization density corresponds to negative ionospheric storms, while positive storms are characterized by significant increases in the ionization density (Zolesi and Cander, 2014). Low latitude ionosphere stations, such as Tucumán, during geomagnetic storms, are subject to very particular effects.

Electric fields induced due to solar wind conditions near Earth can penetrate into the magnetosphere and into the dayside ionosphere near the equator during some geomagnetic storms. These electric fields are called prompt penetrating electric fields (PPEFs). During the most intense magnetic storms, these E can be significantly larger than the electric fields associated with the regular fountain effect near the equatorial upper atmosphere. If the IMF points to the south, leading to a dawn-to-dusk or eastward induced electric field, the consequent superposed E will enhance the regular fountain effect and produce the so-called super-fountain effect. From the combination of solar photoionization and plasma transport, the EIA plasma densities will be enhanced to values above quiet time levels, creating a positive ionospheric storm (Tsurutani et al., 2008).

If these penetrating fields can reach the nightside ionosphere near the equator, the electric field will point to the westward direction. It will be advected together with the ionospheric plasma downward to lower altitudes, with a velocity equal to $E \times B$. The chemical reactions will produce recombination at these low altitudes; this will cause a reduction of the electron density, causing a negative-phase ionospheric storm (Tsurutani et al., 2008).

Figure 3 shows two shaded zones (different periods corresponding to the shaded regions in Figure 1), namely (a) and (b). In case (a), it can be seen that *vTEC* decreases significantly (between 10 and 20 TECu) from the last hours of 6 October until ≈ 06.00 hs UT (02.00 LT) on 7 October in agreement with the main phase of the geomagnetic storm (Figure 1). While

in (b), it can be observed a sudden increase in *vTEC* up to ≈ 24.11 TECu. In this last case, the increment is also observed in coincidence with the more intense geomagnetically disturbed period on 7 October (see Figure 1). Our main hypothesis is that case (a) corresponds to a negative ionospheric storm, according to the LT it is developing at nighttime. Case (b) corresponds to a positive ionospheric storm developing in dayside.

An important observation is that the values are plotted using UT, while to study local/regional behavior LT = UT − 4 should be taken into account (secondary horizontal axis in Figure 3).

Even when *foF2* and *TEC* are the main parameters to study ionospheric storms they do not exhibit always the same characteristics or behavior. The electron density sensitivity towards changes in neutral composition, thermospheric gas temperature, and horizontal winds can be more influential at heights close to the *foF2*. On the other hand, *TEC* is an integrated value along the different ionosphere heights where electrodynamic effects acting at higher altitudes (400 – 800 km), such as PPEFs and plasma fluxes from the plasmasphere may significantly contribute to the TEC value (Zolesi and Cander, 2014).

On 6 October two disturbances in the ionosphere are observed (in Figure 4). In both cases, pre-storm enhancements in *foF2* occur in daytime and nighttime. These pre-storm enhancements of *foF2* (or *NmF2*) have been less studied than the storm time behavior of the F2 region and the mechanisms of these effects remain unknown (e.g. Buresova and Lastovicka, 2007, 2008). We focus our study on the storm onset on 7 October.

We can see a depletion in *foF2* (compared with the reference curve in dashed lines in Figure 4, panel 2), called negative ionospheric storm during the early stage of the storm, approximately from post-sunset to dawn. After several hours with storm-time values close to the reference ones, an increase in *foF2* (positive ionospheric storm) is observed in the afternoon on 7 October, during the last stage of the main phase of the storm.

It should be noted that the main phase of the storm after the first SSC (see Dst in Figure 4 panel 1) is developing almost in coincidence with the negative ionospheric storm which suggests a fast mechanism acting in the ionosphere. Similar behavior can be observed for the second SSC in concordance with the positive ionospheric storm.

3.2.1. Negative Ionospheric Storm

The prompt decrease in *foF2* (Figure 4 panel 2, shaded region (a)) suggests a rapid mechanism such as an electrodynamic one to produce it. We suggest a prompt penetration electric field (PPEF) as a probable mechanism. These transient electric fields have typical lifetimes of about an hour (e.g. Gonzales et al., 1979; Fejer and Scherliess, 1997). An eastward PPEF is highly correlated with the Bz component of the interplanetary magnetic field (Fejer, Scherliess, and de Paula, 1999; Klimenko and Klimenko, 2012) at daytime, while it is westwards during nighttime.

The empirical model of the equatorial electric field (panel 5 in Figure 4), for this cases, shows the presence of electric fields of magnetospheric origin when compared with the reference curve in agreement with our hypothesis.

The PPEF drives the electron density peak of the F2 layer (proportional to *foF2*) rapidly upwards. That produces a reduction of the electron density by the vertical expansion of ionospheric plasma (e.g. Balan et al., 2011). Figure 4 panel 4 shows the variations of the peak height *hmF2* for the storm period considered. It can be seen an increase from about 300 km to values greater than 400 km (roughly speaking) in association with the negative ionospheric storm, which could corroborate the previous assumption.

Figure 5 shows ionograms acquired at 05:10 UT for three consecutive days (6, 7, and 8 October 2015). The acquisition time was selected during the negative ionospheric storm.
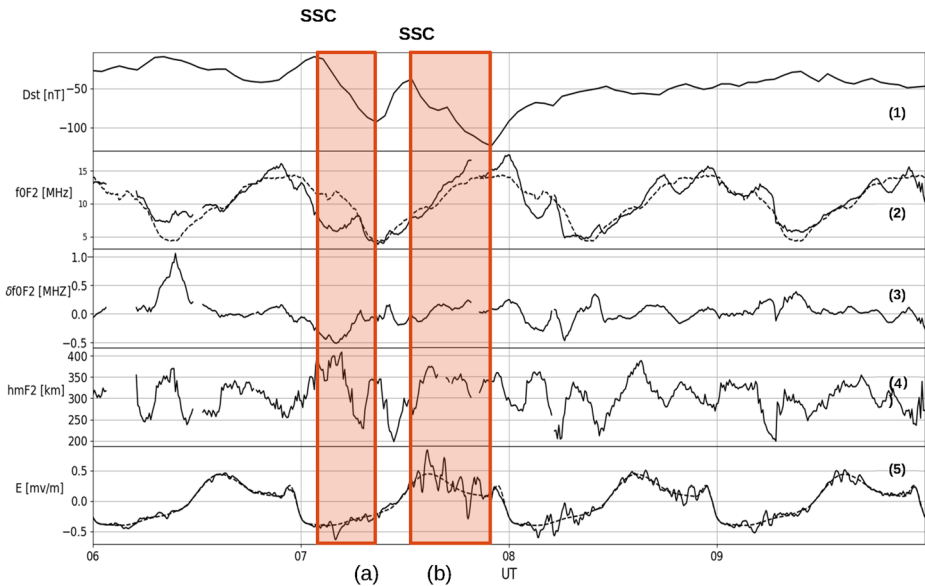
Figure 4 Ionospheric parameters for four days (6 – 9 October 2015) at Tucumán station. The parameters are: panel 1 Dst index, panel 2 critical frequency of the F2 layer *foF2* (bold line) and a reference curve using the five nearest geomagnetically quiet days (dashed line), panel 3 *δfoF2* calculated using the above panel, panel 4 *hmF2* and panel 5 the electric field modeled at the equatorial ionosphere (see Section 2). Shaded regions (**a**) and (**b**) highlight the main phases of both geomagnetic storms developing during 7 October, SSCs are marked as well. The first SSC occurs at 02 UT (22 LT) on 6 October and the second one at 13 UT (09 LT).

As can be observed, the ionosonde allows one to analyze the morphology of the ionosphere during the storm. The initial assumption of the F2 layer uplift using the model (see Equation 1) can be confirmed by observing that F2 height, on 7 October, is uplifted in comparison with the previous and the next days. The Shimazaki formula is a rough approximation that can be used to observe a general behavior of the ionosphere and is useful for space weather products (see Equation 1 and Section 2). It is an empirical model that in this case uses automatically scaled values (which can have substantial differences with the corrected ones).

It is unlikely that a disturbance in the equatorward winds produced the initial decreases in *foF2*. We should observe that *hmF2* enhancements are initiated before *foF2* starts to decrease. There should be a temporary delay between *hmF2* and *foF2* variations, which does not occur in this case study.

3.2.2. Positive Ionospheric Storm

The positive storm effect observed in the afternoon during the final stage of a long main phase (see Figure 4 shaded region (b)) could, potentially, be caused by strong equatorward thermospheric winds. These winds rise the F2 region electron density, by pushing ions and electrons along magnetic field lines from high and middle latitudes to low latitudes (e.g. Goncharenko et al., 2007; Lu et al., 2008). Another possible cause is the down-welling of neutral atomic oxygen at low latitudes as a result of the storm-induced thermospheric circulation (e.g. Buonsanto, 1999; Kane, 2005; Danilov, 2001 and the references therein). A moderate decrease of the N_2 density is also frequently observed (e.g. Mayr, Harris, and Spencer, 1978; Fuller-Rowell et al., 1996). Because several hours are required for the generation and
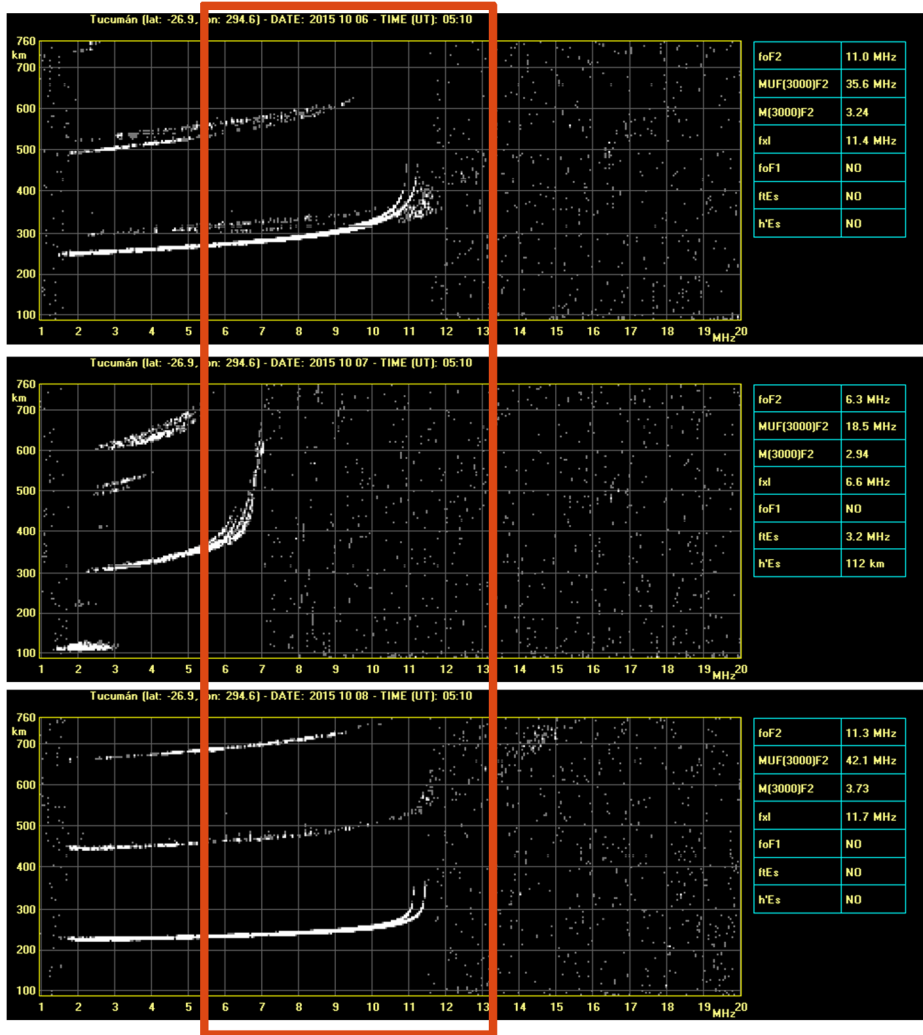
Figure 5 Ionograms acquired at 05:10 UT for three consecutive days (6, 7, and 8 October 2015) at Tucumán.

equatorward propagation of the storm-time thermospheric circulation, these winds could be a plausible mechanism for the positive ionospheric storm effects (related to the geomagnetic disturbances in the early hours of the day).

Unfortunately, no data of neutral gases, molecular nitrogen, and atomic oxygen were available during this storm event, (e.g. Global Ultraviolet Imager (GUVI) data), which prevents analyzing the composition change effects on the ionosphere over Tucumán.

Additionally, it is expected a decrease in the height of the layer (*hmF2*) when N2 is decreased (e.g. Prölss, 1991). Compared with the same hours on 6 October, values slightly enhanced of *hmF2* ($\approx 340-350$ km) are observed in association with the positive storm effect in *foF2* in the afternoon.

In Figure 6, ionograms for three consecutive days at 00:00 UT are shown. The ionogram of 8 October shows the morphology and parameters of the ionosphere during the positive

storm. Let us recall that the minimum Dst observed occurred at 23 UT on 7 October and this ionogram was recorded one hour later when perturbations were still ongoing. An enhancement in *foF2* can be seen very clearly and yet the height of the F2 layer has not been enhanced, when compared with the previous and the next days. This measurement supports our initial hypothesis. It should it be noted that the enhancement of the critical frequency has a severe impact in HF telecommunications, in this case, the enhancement is ≈ 4 MHz. The enhancement persists for several hours, which can be critical for some HF communications.

This could indicate that changes in composition would have little effect on the positive storm effect during this particular event.

The storm-time global circulation produced by the thermospheric winds, which are produced by a large amount of energy deposition into the high-latitude regions of the Earth, generates eastward-directed disturbance dynamo electric fields (Blanc and Richmond, 1980), which can persist for many hours (Maruyama et al., 2007). The dynamo electric field can contribute to the enhancement of the electron density in regions close to the equator. This is because the energy deposition at high latitudes and the beginning of the disturbance dynamo at low latitudes have a delay of the order of $14 - 24$ hours (e.g. Fejer, Larsen, and Farley, 1983). Moreover, it is reasonable to assume an association between electron density and disturbance dynamo because this one occurs around the major enhancement in geomagnetic activity (Scherliess and Fejer, 1997). So, this could be a cause for the positive storm effect during the last stage of the main phase.

An enhancement in *vTEC* behavior is also clearly seen in this stage of the storm (Figure 3 shaded region (b)) when differences between the regular behavior and the perturbed curve reached ≈ 24.11 TECu, which could apply to the above physical mechanism.

In addition to the *foF2* and *vTEC* enhancement, from panel 5 in Figure 4 (shaded region (b)), it can be observed large perturbations in the equatorial electric fields compared with the reference curve. Let us recall that this model uses, as input, data from several instruments (ACE satellite, radar from JULIA, and magnetometer at CHAMP satellite). These observations are consistent with the characteristics of PPEF at equatorial regions when the IMF is southward. This is due to the Earth's magnetic field horizontal at the equator and PPEFs directed eastward, and thus $E \times B$ convection magnitudes are larger (Tsurutani et al., 2008). The equatorial PPEFs at dayside produce the super-fountain effect affecting low latitudes (enhancement in ionization) similar to our case study. As a result, we can conclude that the mechanisms acting in the positive storm are mainly a combination of PPEF and a disturbance dynamo electric field.

4. Discussion and Conclusions

One of the aims of this work was to analyze the chain of coupling processes of an intense geomagnetic storm produced by a not so frequent forcing, analyzing the solar driver, the interplanetary medium, the magnetosphere, and the ionosphere, with especial emphasis in effects over a low latitude station.

We presented a study of the 7 October 2015 intense geomagnetic storm, mainly analyzing its solar causes and ionospheric consequences. From the analysis of solar and interplanetary observations, we identified its solar-interplanetary driver as a coronal hole and its consequent fast/slow solar wind interaction region. We were especially interested in this case study because is not that often (less than 30%) that SIR/HSSs produce intense storms and, moreover, in most cases, a combined SIR/HSSs interacting with an ICME are responsible for the most intense storms associated with CIRs. However, no CME candidates were present in this case
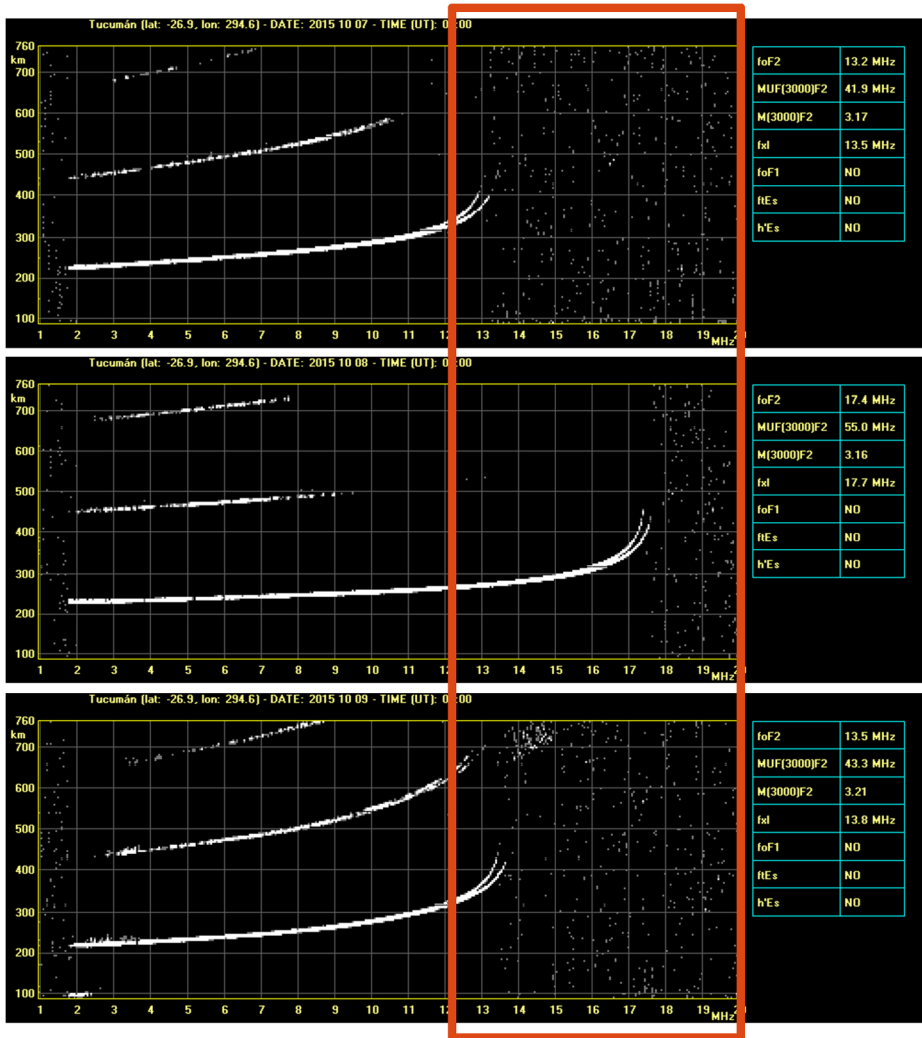
Figure 6 Ionograms acquired in Tucumán at 00:00 UT for three consecutive days (8, 9 and 10 October).

and we found strong evidence that the interplanetary conditions near Earth corresponded to an isolated but complex CIR, presenting three different sub-structures between its front and its end, which produced a two-phase geomagnetic storm (see Figure 1). We confirmed here that, for a better space weather forecast, it is important to analyze the solar source of the solar wind directed to Earth, generating geomagnetic events, as well as to study the interplanetary evolution and interaction of the magnetized plasma traveling from the Sun to the Earth, and its condition when reaching the space near Earth. As a consequence of the two-steps driver, the complex geomagnetic storm had two SSCs. The first one at 02 UT (23 LT on 6 October) followed by the main phase until 6 UT when Dst reached −93 nT (moderate storm). Then a second SSC observed when the storm reached −124 nT at 22 UT (18 LT).

During adverse space weather conditions, the ionosphere can be severely disturbed posing great challenges to space-based technologies such as navigation and positioning and HF

communications systems among other applications (Zolesi and Cander, 2014; among others). The level of disruption in the ionosphere depends, not only on the geomagnetic storm itself (as global phenomena), but also on the local ionosphere.

The variations on relative ionization, loss and transport phenomena produce different changes at different ionospheric heights. The ionosphere is highly variable in time (at different scales: daily, seasonal, and solar cycles) and in space (geographically and geomagnetically) (Zolesi and Cander, 2014). Thus the ionosphere systematic monitoring is key to understand and forecast its dynamics and morphology with space weather purposes.

The most important techniques for this monitoring are based on propagation effects that influence radio waves traveling through the ionosphere. In this work we analyzed the low latitude ionosphere using two of the most widely used instruments: GPS receiver and an ionosonde. We combined measurements from both instruments at the Tucumán low latitude station. The observations showed two ionospheric storms: a negative one (at nighttime) and a positive one (at dayside).

The analysis of the negative storm showed that the penetration of the fast electric field from the magnetosphere (PPEFs) was the main involved mechanism. Typically, PPEFs act almost immediately, while the disturbance dynamo develops more slowly taking several hours and its effects can persist for some hours.

After several hours, the second SSC triggered the positive ionospheric storm with significant *foF2* enhancement that followed the geomagnetic storm main phase development. In this case, the analysis showed a combination of mechanisms responsible for the electron density and critical frequency enhancement. The main mechanisms were PPEFs from the magnetosphere-ionosphere coupling, and the disturbed dynamo electric fields due to the already perturbed system since the first SSC. It must be observed that little effects related to probable changes in composition are likely to be acting in this case.

Based on the analysis of the underlying physical processes responsible for the observed storm-time disturbances, we conclude that the mechanism(s) that predominates in the formation of positive or negative storms depends on the particular geographic region and/or local time, combined with which phase of the particular disturbance occurs.

Summarizing, we have used different instruments, from space and from ground observatories and from different sub-domains where space weather impacts, to analyze a case study, and have identified the detailed influence that a CIR can have on the low latitude ionosphere. The results presented here will help to better understand the full chain of processes which couple the different regions of the space environment of the Earth.

Disclosure of Potential Conflicts of Interest   The authors declare that there are no conflicts of interest.

Publisher's Note   Springer Nature remains neutral with regard to jurisdictional claims in published maps and institutional affiliations.

References

Alves, M.V.: 2006, Geoeffectiveness of coronating interaction regions as measured by index. *J. Geophys. Res.* **111**, 0148. DOI.

Bagiya, M., Krishna, I., Joshi, H., Thampi, S., Tsugawa, T., Ravindran, S., Sridharan, R., Pathan, B.: 2011, Low-latitude ionospheric-thermospheric response to stormtime electrodynamical coupling between high and low latitudes. *J. Geophys. Res.* **116**, A01303. DOI.

Balan, N., Yamamoto, M., Sreeja, V., Batista, I.S., Lynn, K.J.W., Abdu, M.A., Ravindran, S., Kikuchi, T., Otsuka, Y., Shokawa, K., Alex, S.: 2011, A statistical study of the response of the dayside equatorial F2 layer in the main phase of intense geomagnetic storms as an indicator of penetration electric field. *J. Geophys. Res.* **116**, A03323. DOI.

Bianchi, C., Baskaradas, J., Pezzopane, M., Pietrella, M., Umberto, S., Zuccheretti, E.: 2013, Fading in the HF ionospheric channel and the role of irregularities. *Adv. Space Res.* **52**, 403. DOI.

Bilitza, D., Sheik, N., Eyfrig, R.: 1979, A global model for the height of the F2-peak using M3000 values from the CCIR numerical map. *Telecommun. J.* **46**, 549.

Blanc, M., Richmond, A.D.: 1980, The ionospheric disturbance dynamo. *J. Geophys. Res.* **85**, 1669. DOI.

Bothmer, V., Zhukov, A., Daglis, I.: 2007, *The Sun as the Prime Source of Space Weather*, Springer, Berlin. DOI.

Bradley, P.A., Dudeney, J.R.: 1973, A simple model of the vertical distribution of the electron concentration in the ionosphere. *J. Atmos. Terr. Phys.* **35**, 2131. DOI.

Buonsanto, M.J.: 1999, Ionospheric storms, a review. *Space Sci. Rev.* **88**, 563. DOI.

Buresova, D., Lastovicka, J.: 2007, Pre-storm enhancements of foF2 above Europe. *Adv. Space Res.* **39**, 1298. DOI.

Buresova, D., Lastovicka, J.: 2008, Pre-storm electron density enhancements at middle latitudes. *J. Atmos. Solar-Terr. Phys.* **70**, 1848. DOI.

Cabrera, M., Zuccheretti, E., Ezquer, R., Sciacca, U., Lopez, J., Molina, M., Baskaradas, J.: 2010, Some considerations for different time-domain signal processing of pulse compression radar. *Ann. Geophys.* **53**(5–6), 1. DOI.

Chi, Y., Shen, C., Luo, B., Wang, Y., Xu, M.: 2018, Geoeffectiveness of stream interaction regions from 1995 to 2016. *Space Weather* **16**, 1542. DOI.

Danilov, A.D.: 2001, F2-region response to geomagnetic disturbances. *J. Atmos. Solar-Terr. Phys.* **63**, 441. DOI.

Danilov, A.D.: 2013, Ionospheric F-region response to geomagnetic disturbances. *J. Atmos. Solar-Terr. Phys.* **52**(3), 343. DOI.

Dasso, S., Shea, M.A.: 2020, Magnetosphere, ionosphere and their connection to Space Weather. *Adv. Space Res.* **65**, 2081. DOI.

Fejer, B.G., Kamide, Y., Slavi, J.A.: 1986, *Solar Wind-Magnetosphere Coupling*, Terra Scientific Publishing Co., Tokyo, 519.

Fejer, B.G., Larsen, M.F., Farley, D.T.: 1983, Equatorial disturbance dynamo electric fields. *Geophys. Res. Lett.* **10**, 537. DOI.

Fejer, B.G., Scherliess, L.: 1997, Empirical models of storm time equatorial electric fields. *J. Geophys. Res.* **102**, 24,047. DOI.

Fejer, B.G., Scherliess, L., de Paula, E.R.: 1999, Effects of the vertical plasma drift velocity on the generation and evolution of equatorial spread F. *J. Geophys. Res.* **104**(A9), 19,859. DOI.

Fuller-Rowell, T., Codrescu, M., Risbeth, H., Moffett, R., Quegan, S.: 1996, On the seasonal response of the thermosphere and ionosphere to geomagnetic storms. *J. Geophys. Res.* **101**, 2343. DOI.

Fuller-Rowell, T.J., Codrescu, M.V., Roble, R.G., Richmond, A.D.: 1997, How does the thermosphere and ionosphere react to a geomagnetic storm? In: Tsurutani, B.T. (ed.) *Magnetic Storms*, *Geophysical Monograph Series* **98**, Am. Geophys. Union, Washington, 203. DOI.

Fuller-Rowell, T.J., Millward, G.H., Richmond, A.D., Codrescu, M.V.: 2002, Storm-time changes in the upper atmosphere at low latitudes. *J. Atmos. Solar-Terr. Phys.* **64**, 1383. DOI.

Goncharenko, L.P., Foster, J.C., Coster, A.J., Huang, C., Aponte, N., Paxton, L.J.: 2007, Observations of a positive storm phase on September 10, 2005. *J. Atmos. Solar-Terr. Phys.* **69**(10–11), 1253. DOI.

Gonzales, C.A., Kelley, M.C., Fejer, B.G., Vickrey, J.F., Woodman, R.F.: 1979, Equatorial electric fields during magnetically disturbed conditions: 2. Implications of simultaneous auroral and equatorial measurements. *J. Geophys. Res.* **84**(A10), 5803. DOI.

Grandin, M., Aikio, A., Kozlovsky, A.: 2019, Properties and geoeffectiveness of solar wind high-speed streams and stream interaction regions during Solar Cycles 23 and 24. *J. Geophys. Res.* **124**(6), 3871. DOI.

Kamide, Y., Yokoyama, N., Gonzalez, W., Tsurutani, B.T., Daglis, I.A., Brekke, A., Masuda, S.: 1998, Two-step development of geomagnetic storms. *J. Geophys. Res.* **103**, 6917. DOI.

Kane, R.P.: 2005, Ionospheric foF2 anomalies during some intense geomagnetic storms. *Ann. Geophys.* **23**, 2487. DOI.

Kelley, M.C.: 1989, *The Earth's Ionosphere: Plasma Physics and Electrodynamics*, Academic Press, San Diego. DOI.

Kelley, M.C., Fejer, B.G., Gonzales, C.A.: 1979, An explanation for anomalous equatorial ionospheric electric field associated with a northward turning of the interplanetary magnetic field. *Geophys. Res. Lett.* **6**(4), 301. DOI.

Kikuchi, T., Luehr, H., Schlegel, K., Tachihara, H., Shinohara, M., Kitamura, T.-I.: 2000, Penetration of auroral electric fields to the equator during a substorm. *J. Geophys. Res.* **105**(A10), 23,251. DOI.

Kilpua, E., Koskinen, H.E.J., Pulkkinen, T.I.: 2017, *Living Rev. Solar Phys.* **14**, 5. DOI.

Klimenko, M.V., Klimenko, V.V.: 2012, Disturbance dynamo, prompt penetration electric field and over-sheilding in the Earth's ionosphere during geomagnetic storm. *J. Atmos. Solar-Terr. Phys.* **90–91**, 146. DOI.

Krishna, S.G.: 2020, GPS-TEC Analysis Software Version 2.9.5. Available at: http://seemala.blogspot.in (Accessed 01 October 2020).

Lu, G., Goncharenko, L.P., Richmond, A.D., Roble, R.G., Aponte, N.: 2008, A dayside ionospheric positive storm phase driven by neutral winds. *J. Geophys. Res.* **113**, A08304. DOI.

Mannucci, A.J., Tsurutani, B.T., Lijima, B.A., Komjathu, A., Saito, A., Gonzalez, W.D.: 2005, Dayside global ionospheric response to the major interplanetary events of October 29, 2003 "Halloween storms". *Geophys. Res. Lett.* **32**, L12S02. DOI.

Maruyama, N., Richmond, A.D., Fuller-Rowell, T.J., Codrescu, M.V., Sazykin, S., Toffoletto, F.R., Spiro, R.W., Millward, G.H.: 2007, Interaction between direct penetration and disturbance dynamo electric fields in the storm-time equatorial ionosphere. *Geophys. Res. Lett.* **32**, L17105. DOI.

Matsui, H., Erickson, P.J., Foster, J.C., Torbert, R.B., Argall, M.R., Anderson, B.J., Blake, J.B., Cohen, I.J., Ergun, R.E., Farrugia, C.J., Khotyaintsev, Y.V., Korth, H., Lindqvist, P.A., Magnes, W., Marklund, G.T., Mauk, B.H., Paulson, K.W., Russell, C.T., Strangeway, R.J., Turner, D.L.: 2016, Dipolarization in the inner magnetosphere during a geomagnetic storm on 7 October 2015. *Geophys. Res. Lett.* **43**, 9397. DOI.

Mayr, H.G., Harris, I., Spencer, N.W.: 1978, Some properties of upper atmosphere dynamics. *Rev. Geophys. Space Phys.* **16**(4), 539. DOI.

Molina, M.G., Zuccheretti, E., Cabrera, M.A., Bianchi, C., Sciacca, U., Baskaradas, J.: 2016, Automatic ionospheric layers detection: algorithms analysis. *Adv. Space Res.* DOI.

Newell, P.T., Sotirelis, T., Liou, K., Meng, C.I., Rich, F.J.: 2007, A nearly universal solar wind-magnetosphere coupling function inferred from 10 magnetospheric state variables. *J. Geophys. Res.* **112**, 0148. DOI.

Nishida, A., Iwasaki, T., Nagata, T.: 1966, The origin of fluctuations in the equatorial electrojet: a new type of geomagnetic variation. *Ann. Geophys.* **22**, 478.

Prölss, G.W.: 1991, Thermosphere-ionosphere coupling during disturbed conditions. *J. Geomagn. Geoelectr.* **43**, 537. DOI.

Prölss, G.: 2004, *Physics of the Earth's Space Environment*, Springer, Berlin. DOI.

Retterer, J.M., Kelley, M.C.: 2010, Solar wind drivers for low-latitude ionosphere models during geomagnetic storms. *J. Atmos. Solar-Terr. Phys.* **72**, 344. DOI.

Richardson, I.G.: 2018, Solar wind stream interaction regions throughout the heliosphere. *Living Rev. Solar Phys.* **15**, 1. DOI.

Richardson, I.G., Cane, H.V.: 2010, Near-Earth interplanetary coronal mass ejections during Solar Cycle 23 (1996 – 2009): catalog and summary of properties. *Solar Phys.* **264**, 189. DOI.

Richardson, I., Cane, H.: 2012, Solar wind drivers of geomagnetic storms over more than four solar cycles. *J. Space Weather Space Clim.* DOI.

Scherliess, L., Fejer, B.G.: 1997, Storm time dependence of equatorial disturbance dynamo zonal electric fields. *J. Geophys. Res.* **102**(A12), 24,037. DOI.

Shimazaki, T.: 1955, World-wide variations in the height of the maximum electron density of the ionospheric F2 layer. *J. Radio Res. Labs. Japan* **2**(7), 85.

Snyder, C.W., Neugebauer, M., Rao, U.R.: 1963, The solar wind velocity and its correlation with cosmic-ray variations and with solar and geomagnetic activity. *J. Geophys. Res.* **1896**(68), 0148. DOI.

Sunda, S., Vyas, B.M., Khekale, P.V.: 2013, Storm time spatial variations in TEC during moderate geomagnetic storms in extremely low solar activity conditions (2007 – 2009) over Indian region. *Adv. Space Res.* **52**(1), 158. DOI.

Tsurutani, B., Mannucci, A., Lijima, B., Ali Abdu, M., Sobral, J.H.A., Gonzalez, W.: 2004, Global dayside ionospheric uplift and enhancement associated with interplanetary electric fields. *J. Geophys. Res.* **109**, A08302. DOI.

Tsurutani, B., McPherron, R., Gonzalez, W., Lu, G., Gopalswamy, N., Guarnieri, F.: 2006, *Magnetic Storms Caused by Corotating Solar Wind Streams*, *Geophys. Monogr. Ser.* **167**. DOI.

Tsurutani, B.T., Verkhoglyadova, O.P., Mannucci, A.J., Saito, A., Araki, T., Yumoto, K., Tsuda, T., Abdu, M.A., Sobral, J.H.A., Gonzalez, W.D., McCreadie, H., Lakhina, G.S., Vasyliunas, V.M.: 2008, Prompt penetration electric fields (PPEFs) and their ionospheric effects during the great magnetic storm of 30 – 31 October 2003. *J. Geophys. Res.* **113**, A05311. DOI.

Zhang, J., Richardson, I.G., Webb, D.F.: 2008, Interplanetary origin of multiple-dip geomagnetic storms. *J. Geophys. Res.* **113**, 0148. DOI.

Zolesi, B., Cander, J.: 2014, *Ionospheric Prediction and Forecasting*, Springer, Berlin. DOI.